Pramana – J. Phys. (2017) 88: 53
DOI 10.1007/s12043-016-1360-1

A comparative analysis of the density distributions and the structure models of ^{9}Li

M AYGUN

Department of Physics, Bitlis Eren University, 13000, Bitlis, Turkey
E-mail: murata.25@gmail.com; maygun@beu.edu.tr

MS received 9 June 2016; revised 29 August 2016; accepted 5 October 2016; published online 16 February 2017

Abstract. In the present study, we have analysed the elastic scattering cross-section data of ^{9}Li + ^{12}C system at $E_{\text{lab}} = 540$ MeV and ^{9}Li + ^{208}Pb system at $E_{\text{c.m.}} = 28.3$ MeV for some cluster models and various density distributions of the ^{9}Li nucleus. First, we have obtained five different density distributions of the ^{9}Li nucleus to generate real potentials with the help of double-folding model. For these densities, we have calculated the elastic scattering angular distributions. Secondly, using a simple approach, we have investigated some cluster models of the ^{9}Li nucleus consisting of ^{6}He + ^{3}H and ^{8}Li + n systems. We have presented the comparison of elastic scattering angular distributions for each system with each other as well as with the experimental data. Finally, we have given the cross-section values obtained from the theoretical calculations for all the systems studied in this paper.

Keywords. Optical model; elastic scattering.

PACS Nos 24.10.Ht; 25.60.Bx

1. Introduction

Density distribution plays an important role in obtaining microscopic optical potential, in clarifying the elastic scattering of nucleus–nucleus interactions and in identifying the structure of loosely bound nuclei. Also, the cross-section of the nucleus–nucleus scattering is sensitive to the density distributions of the investigated nuclei [1,2]. Density distributions can be obtained via a phenomenological model or a microscopic model [3,4]. By using any one of these density distributions, the real part of the optical potential evaluated in the analysis of the experimental data can be achieved. The double-folding model (DFM) is one of the most preferred methods [5–13] to evaluate the real part of the optical potential. The DFM generates the real part of the optical potential in terms of density distributions of the projectile and the target together with the effective nucleon–nucleon interaction.

In order to analyse the experimental data of the stable nuclei, different density distributions can be found in the literature. Some of these densities are Woods–Saxon (WS)-type density distribution, Fermi (F)-type density distribution, harmonic oscillator (HO)-type density distribution [14,15], etc. On the other hand, the density distributions of the halo nuclei have a long tail and show a more different structure compared to the stable nuclei. As a result, investigation of the density distributions of the nuclei is important. In this work, the ^{9}Li nucleus is chosen to study density distributions. If one does a comprehensive research over the existing density distributions of ^{9}Li in the literature, one cannot find such a study. Hence, we think that a comparative and comprehensive analysis of various density distributions of the ^{9}Li nucleus would be very significant in explaining the interactions with various target nuclei and will be useful to address this deficiency in the literature.

The cluster structure is an important tool to investigate the structure of a nucleus, to constitute different configurations with elements and to understand the processes in nuclear astrophysics [16,17]. ^{9}Li can be thought to be a prominent candidate for cluster studies. For example, it can be assumed that ^{9}Li consists of different structure models such as ^{6}He+^{3}H and ^{8}Li+n [18]. In the present work, we apply a new and different method for explaining the experimental data of the ^{9}Li–nucleus interactions. In this respect, we investigate

the roles of density distributions formed for some cluster models of the ^{9}Li nucleus. Thus, it will be very important and useful in the analysis of different nucleus interactions as well as the ^{9}Li nucleus.

The present study proceeds in two steps. In the first step, different density distributions of ^{9}Li are tested by using the DFM within a microscopic approach. Thus, the elastic scattering angular distributions are obtained theoretically. The similarities and differences among the density distributions are investigated by comparing each other. In the second step, some structure models of ^{9}Li are examined within the framework of the DFM. In this sense, ^{6}He + ^{3}H and ^{8}Li + n models are handled and the elastic scattering angular distributions for each model are obtained. Finally, all the theoretical results are compared with each other as well as with the experimental data.

In the next section, we demonstrate the optical model (OM) calculations, the density distributions and the internal structure parametrization of the ^{9}Li nucleus. In §3, we give theoretical results of the calculations. Section 4 is devoted to our summary and conclusions.

2. Theory

2.1 *The optical model (OM)*

The optical potential can be written in the following form:

$$V_{\text{optical}}(r) = V(r) + iW(r), \tag{1}$$

where $V(r)$ and $W(r)$ are the real and imaginary potentials, respectively. The phenomenological model and the DFM are the methods used to obtain the real potential. In our study, theoretical calculations are conducted by using the DFM. The double-folding potential is achieved via the nuclear matter distributions of both the projectile and the target nuclei together with an effective nucleon–nucleon interaction potential (ν_{NN}). Thus, the double-folding potential is given by

$$V_{\text{double folding}}(\mathbf{r}) = \int d\mathbf{r}_1 \int d\mathbf{r}_2 \rho_{\text{P}}(\mathbf{r}_1)\rho_{\text{T}}(\mathbf{r}_2)\nu_{\text{NN}}(\mathbf{r}_{12}), \tag{2}$$

where $\mathbf{r}_{12} = \mathbf{r} - \mathbf{r}_1 + \mathbf{r}_2$, $\nu_{\text{NN}}(\mathbf{r}_{12})$ is the effective NN interaction, $\rho_{\text{P}}(\mathbf{r}_1)$ and $\rho_{\text{T}}(\mathbf{r}_2)$, respectively, are the density distributions of the projectile and the target nuclei, normalized so that [19]

$$\int \rho_i(\mathbf{r}_i)d\mathbf{r}_i = A_i, \tag{3}$$

where i = P (projectile) or T (target). In order to make a comparative study, we have used five different density distributions for ^{9}Li. All density distributions of ^{9}Li used in the DFM calculations have been normalized to 9 which is the total number of nucleons of ^{9}Li. Each of these densities is explained in the following. On the other hand, the density distribution of ^{12}C target nucleus is attempted using the form

$$\rho_{^{12}\text{C}}(r) = \rho_0(1 + \zeta r^2)\exp(-\xi r^2), \tag{4}$$

where $\rho_0 = 0.1644$ fm^{-3}, $\zeta = 0.4988$ fm^{-2} and $\xi = 0.3741$ fm^{-2} [20,21]. The density of ^{208}Pb, the other target nucleus investigated in our work, is taken from the Hartree–Fock–Bogoliubov (HFB) method based on the BSk2 Skyrme force [22]. In figure 1, the density

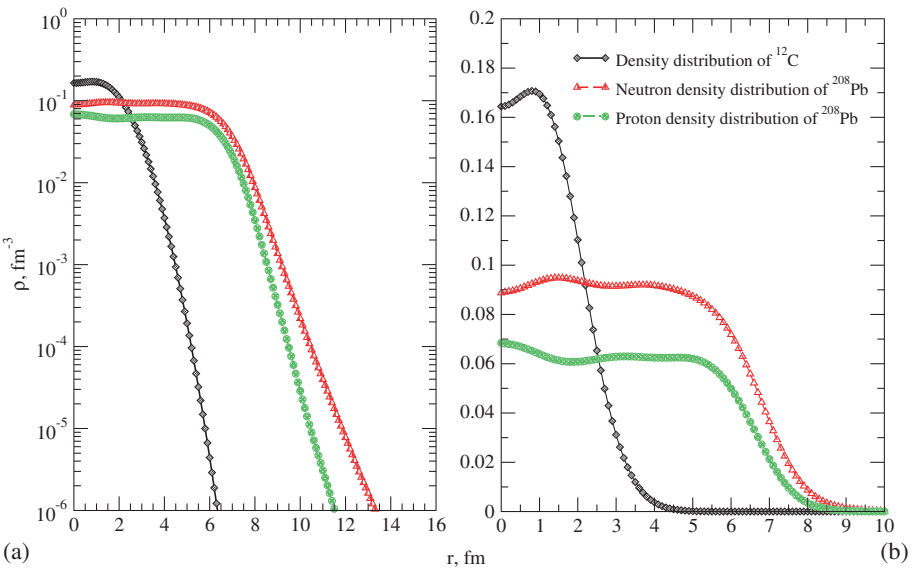

Figure 1. The density distributions of the ^{12}C and ^{208}Pb target nuclei in logarithmic scale (**a**) and linear scale (**b**).

distributions of the target nuclei are plotted on both logarithmic (a) and linear scales (b).

The v_{NN} is integrated over both density distributions. We have used the most common one, the M3Y nucleon–nucleon (Michigan 3 Yukawa) realistic interaction, which is formulated as

$$v_{NN}(r) = 7999\,\frac{\exp(-4r)}{4r} - 2134\,\frac{\exp(-2.5r)}{2.5r} + J_{00}(E)\delta(r), \quad (5)$$

where $J_{00}(E)$ is the exchange term given by

$$J_{00}(E) = 276(1 - 0.005E_{lab}/A_P), \quad (6)$$

where E_{lab} and A_P are the laboratory energy and mass number of the projectile, respectively. Finally, the imaginary part of the optical potential is assumed in the WS form

$$W(r) = W_0 f(r, R_w, a_w), \quad (7)$$

$$f(r, R_w, a_w) = [1+\exp(X)]^{-1}, \quad X = (r - R_w)/a_w, \quad (8)$$

where $R_w = r_w(A_P^{1/3} + A_T^{1/3})$ and A_P and A_T are the mass numbers of the projectile and the target nuclei, respectively.

2.2 *Parametrization of density distributions*

Density distribution used for both the projectile and the target nuclei is very significant to determine the double-folding potential. The densities of the target nuclei have been mentioned before. In this section, ^{9}Li densities are introduced in detail.

2.2.1 *The variational Monte Carlo (VMC) density distribution*. The variational Monte Carlo (VMC) method is applied to construct a variational wave function. Pieper *et al* [4] have reported ^{9}Li density obtained from the VMC calculations using the Argonne v18 (AV18) two-nucleon and Urbana X three-nucleon potentials (AV18+UX). The VMC density is one of the densities investigated in the present work.

2.2.2 *The large-scale shell model (LSSM) density distribution*. Another density which may be used for ^{9}Li is the large-scale shell model (LSSM) density. The LSSM density is acquired by means of a shell-model space by using the WS single-particle wave function basis with realistic exponential asymptotic behaviour [23]. In this manner, Karataglidis *et al* [24] have reported the LSSM density of the ^{9}Li nucleus. As the second density, we examine the microscopic LSSM density of ^{9}Li.

2.2.3 *The Gaussian proton–neutron (GPN) density distribution*. The density distribution of ^{9}Li can be considered as the sum of its constituents densities. In this context, the proton and neutron density distributions of the ^{9}Li nucleus can be taken in the Gaussian forms. Thus, third density evaluated for ^{9}Li is given by [25]

$$\rho_i(r) = N_{ci}\,\frac{1}{\pi^{(3/2)}a^3}\,\exp\left(\frac{-r^2}{a^2}\right), \quad i = p, n, \quad (9)$$

where $N_{cp} = 3$, $N_{cn} = 6$, $a = 1.89$ fm.

2.2.4 *The Gaussian-oscillator (GO) density distribution*. The Gaussian-oscillator (GO) density is the sum of the core (^{8}Li) and the valence (n) densities. While the core density has the Gaussian function as

$$\rho_c(r) = \left(\frac{3}{2\pi R_c^2}\right)^{3/2}\exp\left(-\frac{3r^2}{2R_c^2}\right), \quad (10)$$

the valence density is taken as the 1p-shell harmonic oscillator density formulated by

$$\rho_v(r) = \frac{5}{3}\left(\frac{5}{2\pi R_v^2}\right)^{3/2}\left(\frac{r}{R_v}\right)^2\exp\left(-\frac{5r^2}{2R_v^2}\right), \quad (11)$$

where R_c and R_v are the r.m.s. radii of the core and the valence nucleon distributions, respectively. The total matter distribution ρ_m, normalized to unity [3], is given by

$$\rho_m(r) = [N_c\rho_c(r) + (A - N_c)\rho_v(r)]/A, \quad (12)$$

where N_c and A are the number of nucleons in the core and the mass number, respectively. In our calculations, the values of R_c and R_v are 2.16 fm and 3.22 fm, respectively [26,27].

2.2.5 *The Gaussian density (GD) distribution*. The last investigated density for ^{9}Li is the Gaussian density (GD). This density is assumed to be in the Gaussian form [28]

$$\rho_{^9Li}(r) = \alpha[1 + \beta(r/\gamma)^2]\exp[-(r/\gamma)^2]/\gamma^3, \quad (13)$$

where $\alpha = 0.718$, $\beta = 0.833$ and $\gamma = 1.618$.

2.3 *Parametrization of some structure models of ^{9}Li nucleus*

In this section, some structure models of ^{9}Li have been examined by using a different approach. We have not obtained a new density distribution. We have used the existing density distributions in the literature with only

a simple approach. With this goal, we have taken into consideration several cluster models of ^{9}Li consisting of ^{6}He + ^{3}H and ^{8}Li + n systems. We have used a similar procedure for all the systems analysed in this work. By determining the densities for these models, we have applied the DFM based on the OM to generate the real potential of each system. In this respect, the imaginary part of the optical potential has been taken as the WS potential. Consequently, the nuclear potential for all the theoretical calculations has been assumed in the same form.

2.3.1 *The $^6He + ^3H$ system.* Here we focus on ^{6}He +^{3}H system from cluster models of the ^{9}Li nucleus. According to this simple approach, ^{9}Li density is the sum of the densities of the ^{6}He and ^{3}H nuclei as

$$\rho_{^9\mathrm{Li}}(r) = \rho_{^6\mathrm{He}}(r) + \rho_{^3\mathrm{H}}(r). \tag{14}$$

We can calculate ^{6}He density using the expression

$$\rho_{^6\mathrm{He}}(r) = \rho_0 \exp(-\beta r^2), \tag{15}$$

where β is adjusted to reproduce the experimental value for the r.m.s. radius of ^{6}He (=2.54 fm). ρ_0 can be obtained from the normalization condition

$$\int \rho(r) r^2 \mathrm{d}r = \frac{A}{4\pi}, \tag{16}$$

where A is the mass number. However, ^{3}H density is in VMC density form [4].

2.3.2 *The $^8Li + n$ system.* ^{9}Li nucleus can be of ^{8}Li + n form. In this manner, the density of ^{9}Li is taken as the sum of density distributions of ^{8}Li and n given by

$$\rho_{^9\mathrm{Li}}(r) = \rho_{^8\mathrm{Li}}(r) + \rho_{\mathrm{n}}(r). \tag{17}$$

^{8}Li nuclear matter density is evaluated in the construct [3]

$$\rho_{\mathrm{c}}(r) = \left(\frac{3}{2\pi R_{\mathrm{c}}^2}\right)^{3/2} \exp\left(-\frac{3r^2}{2R_{\mathrm{c}}^2}\right), \tag{18}$$

$$\rho_{\mathrm{v}}(r) = \left(\frac{3}{2\pi R_{\mathrm{v}}^2}\right)^{3/2} \exp\left(-\frac{3r^2}{2R_{\mathrm{v}}^2}\right), \tag{19}$$

where the constant values of R_{c} and R_{v} are 2.50 fm and 2.53 fm, respectively [26]. The total matter distribution ρ_{m}, normalized to unity [3], is formulated by

$$\rho_{\mathrm{m}}(r) = [N_{\mathrm{c}}\rho_{\mathrm{c}}(r) + (A - N_{\mathrm{c}})\rho_{\mathrm{v}}(r)]/A. \tag{20}$$

The density distribution of 1n-halo is in the Gaussian form [29,30]

$$\rho_{\mathrm{n}}(r) = \left(\frac{1}{\gamma\sqrt{\pi}}\right)^3 \exp(-r^2/\gamma^2), \tag{21}$$

where γ is adjusted to reproduce the experimental value for the r.m.s. radius of ^{9}Li.

2.4 *The fitting procedure*

Here, we have introduced the details of fitting procedure used while the density distribution and simple cluster calculations of the ^{9}Li nucleus are performed. In this context, we have investigated the agreement between the theoretical results and the experimental data of ^{9}Li+^{12}C and ^{9}Li+^{208}Pb by searching W_0, r_w and a_w parameters of the imaginary potential used in the DFM calculations. We have conducted a similar fitting procedure for all the systems analysed in this work.

First, we have examined different values of r_w in steps from 0.1 to 0.001 fm. In the density calculations, r_w has been fixed at 0.988 fm for ^{9}Li+^{12}C and at 1.29 fm for ^{9}Li + ^{208}Pb. Then, we have investigated a_w in steps of 0.1 and 0.01 fm at fixed radius and have assumed the value as 0.55 fm for ^{9}Li + ^{12}C and 0.60 fm for ^{9}Li + ^{208}Pb. We have completed the fitting procedure by adjusting the depth of the imaginary potential. All the optical potential parameters are listed in table 1.

Similar to the analysis of the density distributions, we have performed simple cluster model calculations. We have studied different values of r_w in steps from 0.1

Table 1. The optical potential parameters of the VMC, LSSM, GPN, GO and GD density distributions used for the ^{9}Li nucleus in the analysis of the ^{9}Li + ^{12}C and ^{9}Li + ^{208}Pb systems. In all the calculations, the Coulomb radius (R_{C}) is fixed as 1.25.

System	Density distribution	N_R	W (MeV)	r_w (fm)	a_w (fm)	σ (mb)
^{9}Li + ^{12}C	VMC	0.690	28.0	0.988	0.55	885.9
	LSSM	0.675	27.0	0.988	0.55	876.2
	GPN	0.708	29.8	0.988	0.55	900.7
	GO	0.700	28.7	0.988	0.55	891.9
	GD	0.800	36.5	0.988	0.55	949.7
^{9}Li + ^{208}Pb	VMC	1.0	18.2	1.29	0.60	207.8
	LSSM	1.0	16.0	1.29	0.60	203.0
	GPN	1.0	22.2	1.29	0.60	223.2
	GO	1.0	17.5	1.29	0.60	201.0
	GD	1.0	20.8	1.29	0.60	211.4

to 0.001 fm and have accepted r_w as 0.988 fm for ^{9}Li + ^{12}C and 1.31 fm for ^{9}Li + ^{208}Pb. Then, we have evaluated a_w in steps of 0.1 and 0.01 fm at fixed radius and have assumed the value as 0.50 fm for both ^{9}Li + ^{12}C and ^{9}Li + ^{208}Pb systems. Finally, the fitting procedure of the systems has been completed by adjusting the depth of the imaginary potential and all the potential parameters are given in table 2.

The code FRESCO [31] has been used in the DFM calculations. FRESCO, a general-purpose reaction code, is applied to obtain the OM parameters to fit the data [32].

Table 2. The optical potential parameters of the ^{6}He + ^{3}H and ^{8}Li + n systems used for the ^{9}Li nucleus in the analysis of the ^{9}Li + ^{12}C and ^{9}Li + ^{208}Pb systems. In all the calculations, the Coulomb radius (R_C) is fixed as 1.25.

System	Structure model	N_R	W (MeV)	r_w (fm)	a_w (fm)	σ (mb)
^{9}Li + ^{12}C	^{6}He + ^{3}H	0.604	23.6	0.988	0.50	802.5
	^{8}Li + n	0.800	37.6	0.988	0.50	911.4
^{9}Li + ^{208}Pb	^{6}He + ^{3}H	0.870	17.5	1.31	0.50	175.5
	^{8}Li + n	0.660	15.0	1.31	0.50	168.2

3. Results and discussions

3.1 *Analysis of density distributions*

First, we have obtained the density distributions used in the DFM calculations of the ^{9}Li nucleus. We have presented the densities in figure 2 by both logarithmic scale (a) and linear scale (b) in order to make a comparison. It has been observed that the microscopic density of the LSSM model extends much farther when compared with the other densities. The neutron density of the VMC model follows the LSSM density. The GO density is larger than the GPN density. However, the GD and VMC proton density distributions arrive close distance with each other. Also, the density distribution of ^{3}H nucleus used in simple cluster analysis of ^{9}Li is given in both logarithmic scale (a) and linear scale (b) as shown in figure 3.

The optical potential parameters of the investigated densities are listed in table 1. For the ^{9}Li+^{12}C reaction,

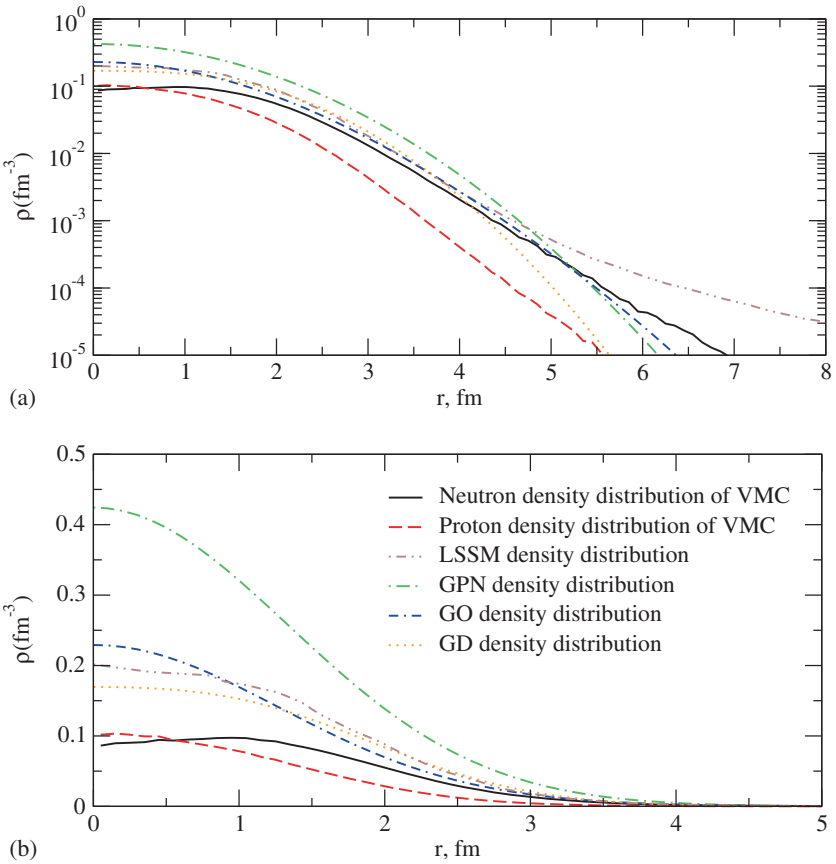

Figure 2. The VMC, LSSM, GPN, GO and GD density distributions of the ^{9}Li nucleus in logarithmic scale (**a**) and linear scale (**b**).

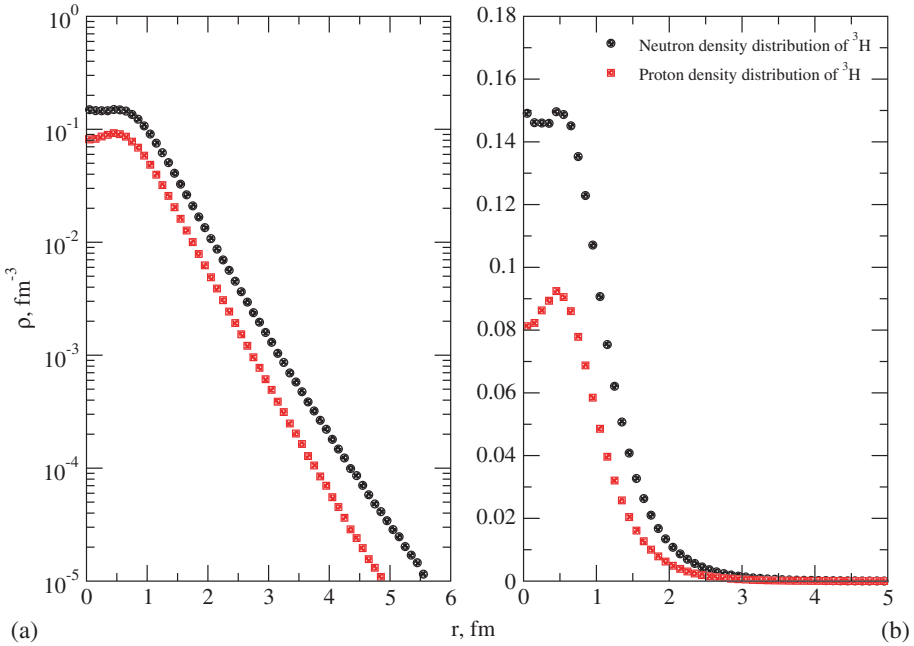

Figure 3. The VMC neutron and proton density distributions of the ^{3}H nucleus in logarithmic scale (**a**) and linear scale (**b**).

it is seen that the imaginary potential depths of the densities are different from each other. The deepest imaginary potential is obtained for the GD density. This state can be attributed to the efficiency of absorption. In the ^{9}Li + ^{208}Pb reaction, the deepest imaginary potential is found for the GPN density. However, we should add that the imaginary potentials of ^{9}Li+^{12}C are deeper than ^{9}Li + ^{208}Pb reaction.

In figure 4, we have plotted the obtained theoretical results to determine the contribution of different density distributions of ^{9}Li in explaining ^{9}Li+^{12}C scattering data at $E_{\text{lab}} = 540$ MeV. We have observed that the DFM results of VMC, LSSM, and GO densities exhibit similar behaviour with each other in general. They have given very compatible results with the data. On the other hand, LSSM results are slightly better than

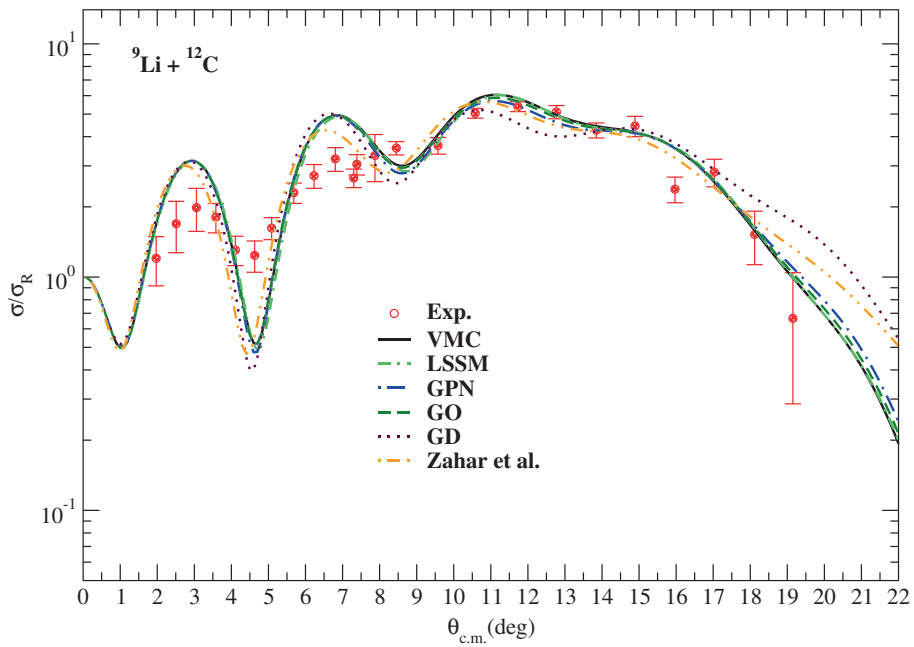

Figure 4. Comparison of elastic scattering angular distributions for the VMC, LSSM, GPN, GO and GD density distributions of the ^{9}Li + ^{12}C reaction with the literature [33] as well as the experimental data at $E_{\text{lab}} = 540$ MeV. The experimental data have been taken from [33].

VMC and GO results. GPN and Gaussian densities have displayed a similar behaviour with each other, but this similarity has been broken down after $\Theta \sim 10°$. However, GPN results are better than GD results. Moreover, Gaussian density has become the weakest density in explaining the scattering data. In addition, our results have been compared with the results of Zahar *et al* [33] which have been obtained by using the OM and the DWBA. While the results of Zahar *et al* [33] have been acquired, we have performed only the phenomenological calculations for the OM parameters given in ref. [33] without including the inelastic scattering of the ^{9}Li nucleus. The theoretical results reported in ref. [33] are the sum of elastic scattering and inelastic scattering. Therefore, we should point out that there is some differences between our results and the results of ref. [33]. As we know, purely elastic scattering data of the ^{9}Li + ^{12}C reaction are not currently available. Therefore, the quasielastic data instead of the elastic scattering data have been used in the fitting procedure.

Then, we have investigated the ^{9}Li + ^{208}Pb system as the interaction with a heavier target nucleus. The elastic scattering data of ^{9}Li + ^{208}Pb system at an incident energy of $E_{\text{c.m.}} = 28.3$ MeV have been measured by Cubero *et al* [34]. In figure 5, we have shown the elastic scattering angular distributions for different densities of ^{9}Li at $E_{\text{c.m.}} = 28.3$ MeV. When the results are compared with each other as well as with the experimental data, it is observed that each of the examined density distributions describes the data well in general. However, it is noticed that the LSSM density distribution explains the data better than the other density distributions. Also, it is better in determining the oscillations of the experimental data.

3.2 *Analysis of the internal structure models*

It is well known that the cluster or internal structure models of the nuclei play important roles in explaining the nucleus–nucleus interactions. The structure models of the nucleus are detailed according to their structure. With this goal, by using a different approach, we have investigated some structure models of the ^{9}Li nucleus in terms of both light and heavy nucleus reactions such as ^{9}Li + ^{12}C and ^{9}Li + ^{208}Pb. The structure models discussed for ^{9}Li in our study consist of ^{6}He + ^{3}H and ^{8}Li + n systems and the optical potential parameters for these models are given in table 2. In ^{9}Li + ^{12}C systems, the potential depths are different from each other. The deepest potential is found for the ^{8}Li + n system. This state can be attributed to the efficiency of absorption. For ^{9}Li + ^{208}Pb, it is seen that the imaginary potential depths are close to each other. However, the deepest potential is obtained for ^{6}He + ^{3}H model.

In figure 6, we have presented the theoretical results of ^{9}Li + ^{12}C reaction. The results of ^{6}He + ^{3}H and ^{8}Li + n systems are different from each other. Also, we can say that the results of ^{6}He + ^{3}H system is slightly better than the results of ^{8}Li + n. We should add

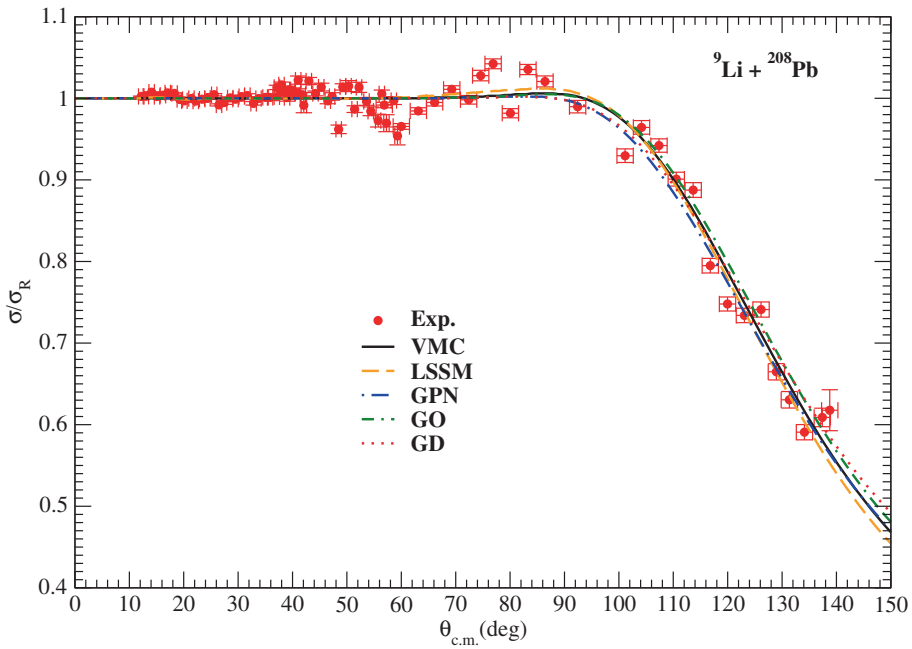

Figure 5. Comparison of elastic scattering angular distributions for the VMC, LSSM, GPN, GO and GD density distributions of the ^{9}Li + ^{208}Pb reaction with the experimental data at $E_{\text{c.m.}} = 28.3$ MeV. The experimental data have been taken from [34].

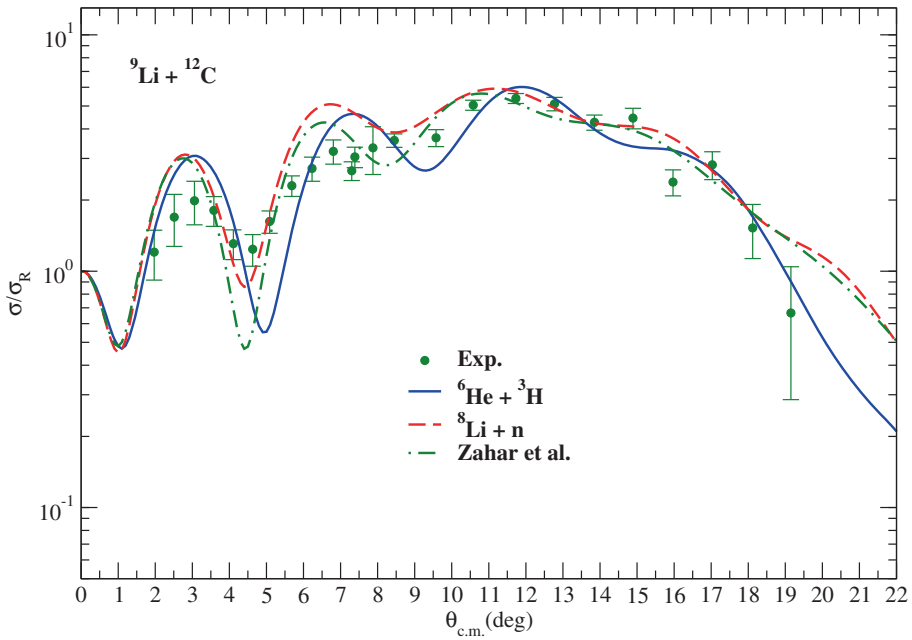

Figure 6. The elastic scattering angular distributions for the ^{6}He + ^{3}H and ^{8}Li + n systems used for the ^{9}Li nucleus in the analysis of the ^{9}Li + ^{12}C system in comparison with the literature [33] and the experimental data.

that none of the investigated structure models of ^{9}Li are very compatible with the experimental data. Additionally, we have compared the best analysis results of both density distributions and structure models of ^{9}Li together with the experimental data and the literature in figure 7. We have observed that none of the results from structure model calculations are much better than the results from the density distribution calculations. We can conclude that simple cluster model does not have a very significant effect on light target nucleus interaction of ^{9}Li with ^{12}C.

In figure 8, we have shown the elastic scattering angular distributions for different structure models of ^{9}Li scattered from ^{208}Pb. The simple cluster results of

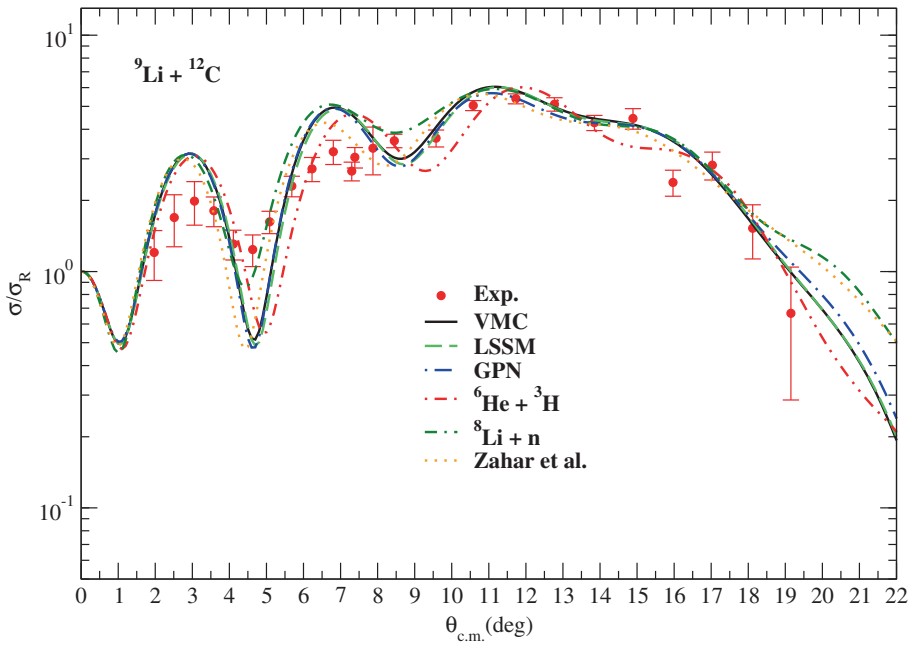

Figure 7. A comparison with the literature [33] and the experimental data of good consistent elastic scattering angular distributions obtained from different density distributions and different structure models used for the ^{9}Li nucleus in the analysis of the ^{9}Li + ^{12}C system.

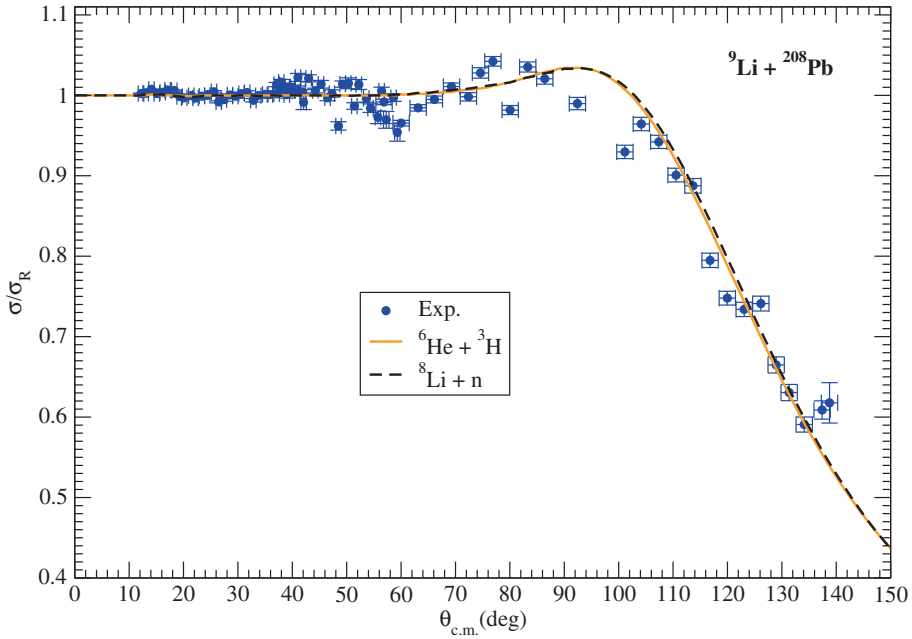

Figure 8. The elastic scattering angular distributions for the ^{6}He + ^{3}H and ^{8}Li + n systems used for the ^{9}Li nucleus in the analysis of the ^{9}Li + ^{208}Pb system.

^{6}He + ^{3}H and ^{8}Li + n are very successful in explaining the experimental data. As a result, we have noticed that the simple cluster model of ^{9}Li interacting with ^{208}Pb heavy target nucleus has an important effect on the elastic scattering results. In figure 9, we have compared the best results of the density distribution and structure model calculations of ^{9}Li with the data. We have observed that while the simple cluster results show a hump structure in the regions of $70° \leq \Theta \leq 100°$, none of the densities provide such a structure. We consider that this result would be important and interesting in the analysis of the ^{9}Li + ^{208}Pb reaction.

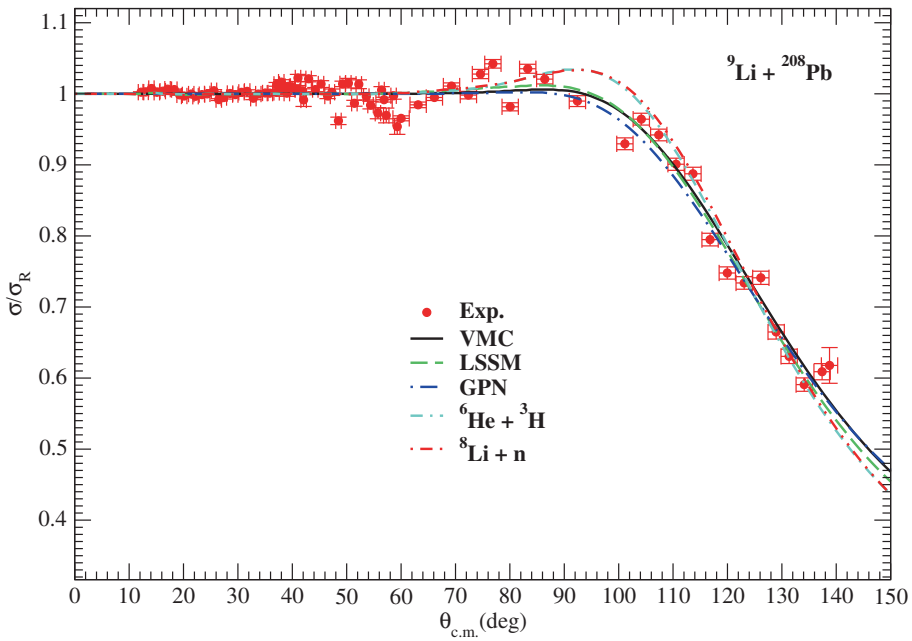

Figure 9. A comparison of good consistent elastic scattering angular distributions with the experimental data obtained from different density distributions and different structure models used for the ^{9}Li nucleus in the analysis of the ^{9}Li + ^{208}Pb system.

3.3 *Analysis of the real and imaginary potentials*

In figures 10 and 11, we have presented the real and imaginary potentials of various density distributions and some structure models of ^{9}Li on ^{12}C and ^{208}Pb. From these results, we have observed that the real potentials of both ^{12}C and ^{208}Pb exhibit similar features. However, the real potentials of ^{9}Li + ^{208}Pb are deeper than the real potentials of ^{9}Li + ^{12}C because ^{208}Pb nucleus is heavier. When we examine the imaginary potential values of ^{9}Li + ^{12}C, ^{208}Pb systems, we have observed that the difference between potential depths is sufficiently clear. This is because of the different

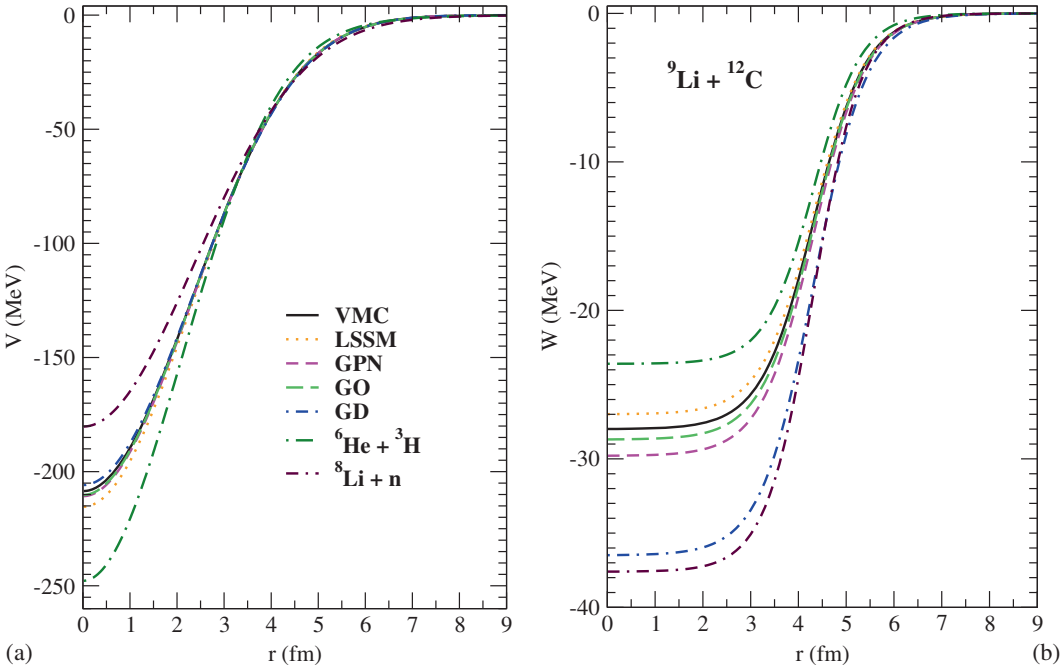

Figure 10. The shapes of the real (**a**) and imaginary potentials (**b**) of the ^{9}Li + ^{12}C reaction for both the VMC, LSSM, GPN, GO, GD density distributions and the ^{6}He + ^{3}H and ^{8}Li + n systems.

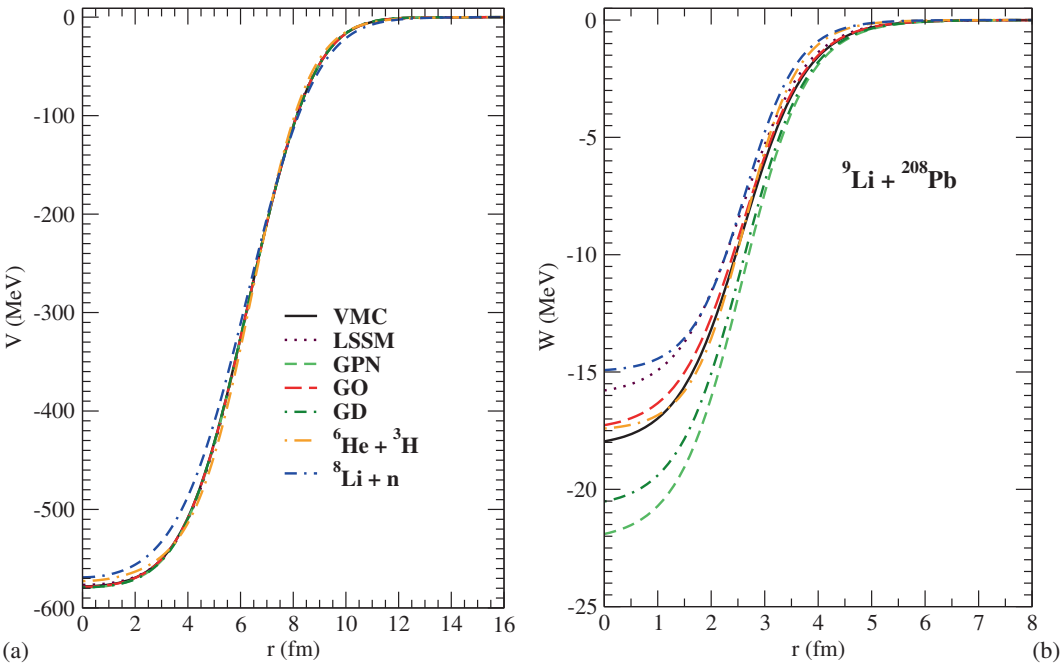

Figure 11. The shapes of the real (**a**) and imaginary potentials (**b**) of the ^{9}Li + ^{208}Pb reaction for both the VMC, LSSM, GPN, GO, GD density distributions and the ^{6}He + ^{3}H and ^{8}Li + n systems.

W values used in the folding model calculations of the density distributions.

3.4 *Analysis of the normalization (N_R) constant*

Here, we discuss the change of normalization (N_R) used in the double-folding calculations. N_R is used to obtain results which are in good agreement with the experimental data. In this respect, $N_R = 1.0$ indicates the success of the DFM [5]. On the other hand, the fact that the value of N_R is different from unity, which means that the model would need corrections, is attributed to strangeness and uncertainties in the data or to uncertainties in the fitting procedures applied or to uncertainties in the densities calculated under the folding-model approach [5].

The values of N_R used in the analysis of the density distributions and the internal structure models of ^{9}Li by ^{12}C and ^{208}Pb are listed in tables 1 and 2. The N_R values of ^{9}Li + ^{12}C have shown deflection from unity. For the ^{9}Li + ^{208}Pb system, while the N_R values of simple cluster model deflect from unity, the N_R values of density distributions are unity. It has been observed that the simple cluster results of ^{208}Pb are in more agreement with the experimental data than to the simple cluster results of ^{12}C although the values of N_R in the structure model calculations of both ^{12}C and ^{208}Pb show deflection from unity. The reason for this, according to us, is that a heavy target nucleus such as ^{208}Pb becomes more effective in the simple cluster analysis of ^{9}Li.

4. Summary and conclusions

In the present study, we have reanalysed the elastic scattering data of the ^{9}Li + ^{12}C system at $E_{\text{lab}} = 540$ MeV and the ^{9}Li + ^{208}Pb system at $E_{\text{c.m.}} = 28.3$ MeV, aiming to address the consistency of different density distributions and some cluster models of the ^{9}Li nucleus. The double-folding potentials generated by using five different densities of ^{9}Li nucleus have been applied to acquire theoretical cross-sections. It has been observed that the results are in good agreement with the experimental data. Moreover, it is seen that this agreement is better than the literature results.

Then, some cluster models of ^{9}Li scattered from the ^{12}C and ^{208}Pb nuclei have been investigated. With this goal, a different and simple method has been applied in the theoretical calculations. It has been observed that simple cluster results of ^{9}Li + ^{12}C reaction do not make a very important contribution to density distribution results of ^{9}Li + ^{12}C, whereas, simple cluster results of ^{9}Li + ^{208}Pb system have presented the differences from density distribution results of ^{9}Li + ^{208}Pb. In addition to this, simple cluster results of ^{9}Li + ^{208}Pb system have shown a hump structure similar to the experimental data in the regions of $70° \leq \Theta \leq 100°$. But, this state has not been observed in the results of density distributions. As a result, we consider that Coulomb scattering of a heavy target nucleus such as ^{208}Pb may be dominant.

Consequently, this work has provided a comprehensive analysis on the validity of five different density distributions of the ^{9}Li nucleus and these densities have given results which are better than the results from the previous studies. In addition to this, a simple model has been used to examine some cluster states of ^{9}Li, and it has been seen that this method has given important results. Therefore, we consider that this method would be useful and interesting in different nucleus states.

Acknowledgements

Author would like to thank the referee for the valuable comments. The author would also like to thank M J G Borge and A M Moro for providing experimental data of the ^{9}Li + ^{208}Pb reaction and H M Maridi and M Y H Farag for providing matter density distributions of the ^{9}Li nucleus for the LSSM model.

References

[1] G D Alkhazov and V V Sarantsev, *Phys. At. Nucl.* **75**, 1544 (2012)
[2] M P Bush, J S Al-Khalili, J A Tostevin and R C Johnson, *Phys. Rev. C* **53**, 3009 (1996)
[3] G D Alkhazov *et al*, *Nucl. Phys. A* **712**, 269 (2002)
[4] S C Pieper, K Varga and R B Wiringa, *Phys. Rev. C* **66**, 044310 (2002)
[5] G R Satchler and W G Love, *Phys. Rep.* **55**, 183 (1979)
[6] M Aygun, *Eur. Phys. J. A* **48**, 145 (2012)
[7] M Aygun, I Boztosun and Y Sahin, *Phys. At. Nucl.* **75**, 963 (2012)
[8] M Aygun, I Boztosun and K Rusek, *Mod. Phys. Lett. A* **28**, 1350112 (2013)
[9] M Aygun, *Ann. Nucl. Energy* **51**, 1 (2013)
[10] M Aygun, *Commun. Theor. Phys.* **60**, 69 (2013)
[11] M Aygun and I Boztosun, *Few-Body Syst.* **55**, 203 (2014)
[12] M Aygun, *J. Korean Phys. Soc.* **66**, 1816 (2015)
[13] M Aygun, *Chin. J. Phys.* **53**, 080301 (2015)
[14] A Ozawa, T Suzuki and I Tanihata, *Nucl. Phys. A* **693**, 32 (2001)
[15] I Tanihata, H Savajols and R Kanungo, *Prog. Part. Nucl. Phys.* **68**, 215 (2013)
[16] F Hoyle, *Astrophys. J. (Suppl.)* **1**, 12 (1954)
[17] Z H Yang *et al*, *Phys. Rev. C* **91**, 024304 (2015)

[18] K Varga, Y Suzuki and I Tanihata, *Phys. Rev. C* **52**, 3013 (1995)
[19] M E Brandan and G R Satchler, *Phys. Rep.* **285**, 143 (1997)
[20] M El-Azab Farid and M A Hassanain, *Nucl. Phys. A* **678**, 39 (2000)
[21] M Karakoc and I Boztosun, *Phys. Rev. C* **73**, 047601 (2006)
[22] Reference Input Parameter Library (RIPL-3), http://www-nds.iaea.org/RIPL-3/
[23] M Y H Farag, E H Esmael and H M Maridi, *Phys. Rev. C* **88**, 064602 (2013)
[24] S Karataglidis, P J Dortmans, K Amos and C Bennhold, *Phys. Rev. C* **61**, 024319 (2000)
[25] A A Korsheninnikov *et al*, *Nucl. Phys. A* **616**, 189c-200c (1997)
[26] A V Dobrovolsky *et al*, *Nucl. Phys. A* **766**, 124 (2006)
[27] S Ilieva *et al*, *Nucl. Phys. A* **875**, 8 (2012)
[28] R Kanungo and C Samanta, *Nucl. Phys. A* **617**, 265 (1997)
[29] A K Chaudhuri, *Phys. Rev. C* **49**, 1603 (1994)
[30] R A Rego, *Nucl. Phys. A* **581**, 119 (1995)
[31] I J Thompson, *Comp. Phys. Rep.* **7**, 167 (1988)
[32] M Aygun, *Acta Phys. Pol. B* **45**, 1875 (2014)
[33] M Zahar *et al*, *Phys. Rev. C* **54**, 1262 (1996)
[34] M Cubero *et al*, *Phys. Rev. Lett.* **109**, 262701 (2012)